

Younger Dryas Age Advance of Franz Josef Glacier in the Southern Alps of New Zealand

G. H. Denton and C. H. Hendy

A corrected radiocarbon age of $11,050 \pm 14$ years before present for an advance of the Franz Josef Glacier to the Waiho Loop terminal moraine on the western flank of New Zealand's Southern Alps shows that glacier advance on a South Pacific island was synchronous with initiation of the Younger Dryas in the North Atlantic region. Hence, cooling at the beginning of the Younger Dryas probably reflects global rather than regional forcing. The source for Younger Dryas climatic cooling may thus lie in the atmosphere rather than in a North Atlantic thermohaline switch.

The Younger Dryas cooling was a short-lived climatic reversal [$\sim 10,000$ to $11,000$ ^{14}C years before present (B.P.)] superimposed on the last deglaciation. It featured rapid shifts of North Atlantic atmospheric temperature (1–5), surface ocean circulation (6), and perhaps thermohaline overturn (7). One proposed explanation is that a temporary shutdown of thermohaline circulation reduced delivery of ocean heat to the North Atlantic and thus led to regional cooling (8). But indications of a Younger Dryas age event in localities far from the North Atlantic Ocean imply that any explanation must address widespread climatic change (9). For example, isotope values in cores from the Sulu Sea in the western tropical Pacific Ocean (10, 11) and off Japan in the northern Pacific Ocean (12) show a return toward glacial values coincident with the beginning of Younger Dryas cooling in the North Atlantic region. Further evidence for Younger Dryas cooling comes from the Gulf of Mexico (13), the Gulf of California (14), and possibly Antarctica (15). Moreover, a lacustrine record from the tropics in East Africa (16) shows that late-glacial climate change was synchronous at high and low latitudes in the Northern Hemisphere, including the Younger Dryas reversal. Here we present a chronology of a glacier advance in New Zealand that allows interhemispheric comparison with classic Younger Dryas cooling in the opposite North Atlantic sector of the globe.

The Franz Josef Glacier (area 37 km^2 ; volume 3.5 km^3 ; mean depth 98 m) flows for 10.7 km down the steep northwest flank of the Southern Alps (Fig. 1) (17, 18). Its head is at 3000 m at the main mountain divide, and it terminates at 290 m in a narrow tongue between precipitous valley walls. It lies at southern mid-latitudes (terminus at $43^\circ 27' \text{S}$; $170^\circ 10' \text{E}$) in the path of

westerlies that deliver enormous amounts of precipitation (5 to 8 m of H_2O per year); the activity gradient is steep; ice flow is rapid; and response time to climatic change is short (< 5 years) (17). Trees now grow to an elevation of 1200 m and cling where possible to steep valley walls above the narrow glacier tongue.

At the last glacial maximum the Franz Josef formed part of a piedmont glacier system on the narrow coastal plain northwest of the Alpine fault (Fig. 1). Moraines of the Okarito and Moana formations mark the Kumara 2₂ ($\sim 18,000$ to $22,300$ ^{14}C years B.P.) and Kumara 3₂ ($\sim 14,000$ to $15,000$ ^{14}C years B.P.) ice limits, respectively, of the last glacial maximum (Fig. 1) (19–24).

Deposited by the Franz Josef Glacier, the Waiho Loop terminal moraine (25, 26) lies about 20 km behind the Kumara 2₂ ice limit and 8 km beyond the Little Ice Age limit (Fig. 1). This terminal loop is the most conspicuous late-glacial moraine in the Southern Alps (Fig. 2). It represents a marked readvance of Franz Josef Glacier that interrupted massive ice recession from the Kumara 3₂ limit.

We focused our study on the stratigraphic section at Canavan Knob (26, 27), a bedrock outcrop that lies 1.6 km upvalley from the Waiho Loop moraine and is surrounded by outwash. The section is best exposed at the eastern corner of an extensive borrow pit on the western slope of the knob. This exposure reveals a conformable sequence from top to bottom consisting of compact till (3.2 m), gray laminated silt (0.08 m), laminated silt and organic silt (0.03 m), wood-bearing diamicton (0.5 m), interbedded silt and organic silt (0.15 m), organic silt (0.05 m), and granite bedrock (Fig. 1). The till is a sandy, gravelly diamicton. Clasts are predominantly granite, graywacke, and schist. Many have shapes indicative of glacial transport and 45% show surface striations. The till unit exhibits apparent bedding or stacking, which dips westward and is most prominent at the base. The wood-bearing diamicton consists

of massive gray silt with enclosed striated gravel clasts and abundant wood pieces. The wood pieces vary greatly in length and orientation, display broken and worn ends, and are of several species (Table 1). None is in place.

We obtained radiocarbon dates from several units of the Canavan Knob stratigraphic section (Table 1) (28). One radiocarbon date shows that the basal organic silt is $11,740$ ^{14}C years old. Thirty-six radiocarbon analyses were performed at three laboratories on 25 individual wood samples from the wood-bearing diamicton. The holocellulose fraction was dated in all cases and duplicate pairs agreed closely. The average of all these dates is $11,140 \pm 200$ ^{14}C years B.P. If it is assumed that all the wood samples are of the same age, calculation of an error-weighted mean age yields a result of $11,150 \pm 14$ ^{14}C years B.P.

We interpret the stratigraphic section as representing an advance of Franz Josef Glacier over Canavan Knob at $11,150 \pm 14$ ^{14}C years B.P. (uncorrected for wood transport time). On the lee side of Canavan Knob, a topographic depression with organic silt and standing water was infilled by gravity flows of till from the advancing glacier snout. The lowest flow incorporated fine-grained sediments that encased and protected the enclosed wood pieces. Subsequent repetition of gravelly flows of till produced the appearance of stacking within the overall till unit. Compaction of the till unit suggests that the glacier then overrode the sequence.

The source of the wood-bearing diamicton is central to this interpretation. From the modern situations at the Franz Josef terminus and the Fox Glacier terminus (which is 13 km southwest of the Franz Josef terminus; Fig. 1), we infer that the battered and broken late-glacial pieces of wood at Canavan Knob were originally swept by avalanches or mass wasting from the steep inner valley walls onto the Franz Josef ice tongue. Those wood pieces, mixed with surficial morainal debris, were carried on the glacier surface 8 km to Canavan Knob where they were incorporated in a debris flow off the advancing glacier snout, which then overran the sample site. Radiocarbon measurements show that wood samples on the present-day Franz Josef ice tongue and on recent ice-cored drift of the Fox Glacier contain ^{14}C attributed to atmospheric testing, indicative of a delay of no more than 30 years between incorporation of ^{14}C and deposition on the ice tongues (Table 1). On the basis of the modern flow rates of Franz Josef Glacier, we estimate that the transit time from the inner valley to Canavan Knob was ≤ 100 years. The radiocarbon dates of the broken and worn wood fragments at Canavan Knob are so

G. H. Denton, Department of Geological Sciences and Institute for Quaternary Studies, University of Maine, Orono, Maine 04469, USA.

C. H. Hendy, Department of Chemistry, University of Waikato, Hamilton, New Zealand.

tightly clustered that anomalously old wood cannot have been included in the sample. Also, tree-ring counts show that the dated wood pieces were short-lived; hence, we avoided the problem of dating center wood from long-lived trees. Finally, rapid glacier flow would have quickly conveyed the surface wood pieces out of Franz Josef valley, precluding mixtures of wood of greatly differing ages. We therefore conclude that the wood-bearing diamicton at the Canavan Knob was likely deposited as a debris flow directly from the advancing Franz Josef Glacier and that 100 years is an appropriate correction for wood-transport time. That correction for transport time would place the advance of Franz Josef Glacier over Canavan Knob at $11,050 \pm 14$ ^{14}C years B.P.

We cannot preclude the possibility that the wood was derived from the Franz Josef outwash plain or on Canavan Knob itself. For example, *Leptospermum scoparium*, which occurs in the wood-bearing diamicton, is today confined to old alluvial surfaces northwest of the Alpine fault (29). Incorporation of wood from either of these two sources would shorten the correction time for wood transport. We do not favor these two alternatives, however, because reworked outwash gravel is not evident in the section and because the battered wood pieces resemble those on present-day glacier surfaces.

Wardle (25) and Mercer (27) concluded that the late-glacial advance of the Franz Josef Glacier over Canavan Knob and the wood-bearing diamicton culminated at the Waiho Loop terminal moraine. Other possibilities are unlikely. If the recorded advance over the Canavan Knob was younger than the Waiho Loop, then its terminal moraine (which could only have been constructed inside the Waiho Loop) would have to have been eroded completely by outwash streams while the Waiho Loop moraine remained intact. The geometry of the Waiho Loop, Canavan Knob, and associated outwash plains precludes this possibility. If it was older than the wood-bearing diamicton at Canavan Knob, the advance to the Waiho Loop would have left no stratigraphic record at Canavan Knob. In this case the terminal moraine of a younger advance over Canavan Knob would then have to have been eroded completely in the same setting that allowed the Waiho Loop to remain intact.

A key to paleoclimatic interpretations from the Canavan Knob stratigraphic section is whether the Waiho Loop moraine represents an advance that was widespread in the Southern Alps. This will prove difficult to determine, because the combination of a preserved terminal moraine and a bedrock knob with exposed glacial deposits, both surrounded by the same outwash plain in the valley center, appears to be

unique. Elsewhere in New Zealand only remnants of late-glacial moraines occur alongside outwash trains on valley floors, and such remnants are generally undated. A conspicuous exception is at Cropp River, 80 km northeast of the Franz Josef Glacier, where wood in a lateral moraine remnant has been radiocarbon dated to 10,250 years B.P. (30). On the other hand, there is no reason to suppose that the Franz Josef Glacier exhibited abnormal response to climatic change, because it deposited the standard Kumara 2_2 and 3_2 drifts (19) as well as typical Little Ice Age moraines (25). Furthermore, surging glaciers have not been reported in New Zealand (31), and in any case they are not thought to deposit classic terminal moraines such as the Waiho Loop (27).

A key to understanding the cause of the Younger Dryas climate reversal is whether its expression was regional or global. A sharp onset of Younger Dryas cooling has been documented in Greenland (1, 4, 5), the North Atlantic Ocean (6), and Europe (2, 3). The most accurate radiocarbon dates in the North Atlantic Ocean are 11,010 to 11,200 ^{14}C years B.P. from cores SU81-18 (32) and Troll 3.1 (6). In southern Sweden, optimal allocation of 25 radiocarbon dates of the sharp change in total pollen influx and in decreasing tree pollen yielded an age of $11,021 \pm 25$ ^{14}C years B.P. (33). Numerous radiocarbon dates of moraines in

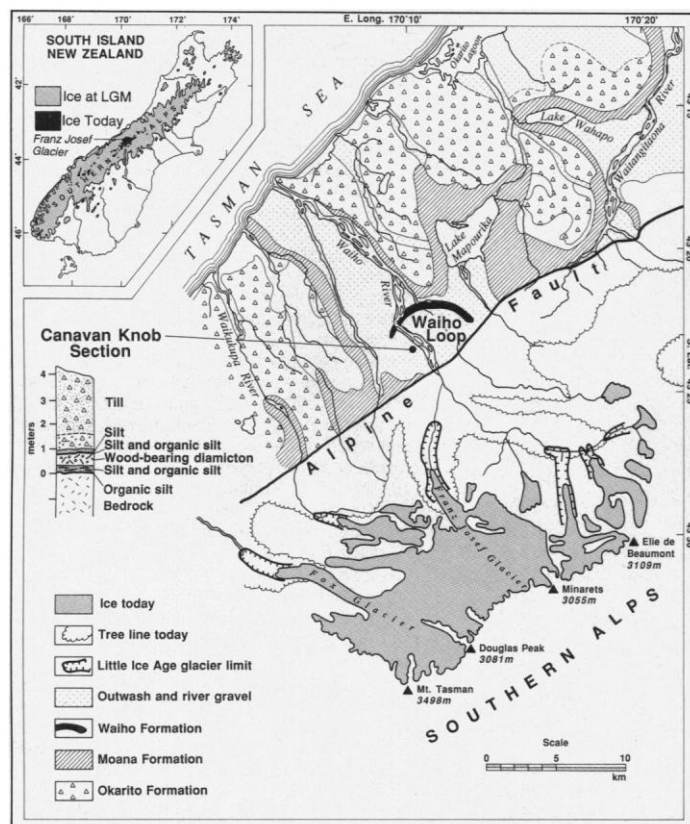


Fig. 1 (left). Position of the Waiho Loop terminal moraine and Canavan Knob stratigraphic section relative to the Okarito and Moana formations of the last glacial maximum [from (19)], Little Ice Age limits (29), and the modern Franz Josef Glacier. The inset shows ice extent at the last glacial maximum in the Southern Alps (35). Massive glacial deposits of the Okarito, Moana, and Waiho formations are preserved on the narrow coastal plain northwest of the Alpine fault. Glacial deposits are rarely preserved in the steep mountain terrain southeast of the Alpine fault. **Fig. 2 (above).** Oblique aerial photo of the Waiho Loop terminal moraine. View is toward the east. The moraine ridge (tree covered) stands 30 to 40 m above the outwash plain (cleared of trees). The distal slope of the moraine ridge is to the left, the proximal slope to the right.

Norway show that the first significant Younger Dryas readvance of the Scandinavian Ice Sheet took place 11,000 ¹⁴C years B.P. (34). Thus the advance of Franz Josef Glacier across Canavan Knob to the Waiho Loop moraine at 11,050 ± 14 ¹⁴C years B.P. coincided with the initial Younger

Dryas climatic deterioration in the North Atlantic region. The implication is that an atmospheric climate signal was registered simultaneously in both polar hemispheres at the beginning of the Younger Dryas. This synchronicity is difficult to explain by a switch in North Atlantic deep-water pro-

duction that does not precede the inter-hemispheric atmospheric signal. Rather, it is more likely that the source of Younger Dryas cooling lies in the atmosphere, perhaps outside the North Atlantic region.

Table 1. Radiocarbon dates from the University of Arizona Radiocarbon Laboratory (A), the University of Waikato Radiocarbon Laboratory (Wk), and the NSF-Arizona AMS Facility (AA). All samples are wood except 92-7. Ages for samples from Franz Josef Glacier and Fox Glacier are mean ages for percent modern carbon, given in parentheses. The holocellulose fraction was dated in all cases but sample 92-7. The wood pieces from Canavan Knob were largely tree stems 11 to 80 cm long, showed broken and worn ends, had rare roots, and were largely devoid of bark. They showed no obvious preferred orientation within the wood-bearing diamicton. The wood pieces collected from debris on the surface of Franz Josef Glacier were tree stems 55 to 65 cm long, showed broken and worn ends, and were largely free of bark. The wood pieces from Fox Glacier were collected from debris on the surface of ice-cored drift isolated from the receding glacier in A.D. 1975. They were derived from the former surface of Fox Glacier. The pieces were tree stems 30 to 120 cm long; showed broken and worn ends, and were largely free of bark. Lab no., laboratory number; δ¹³C is in per mil.

Sample	Lab no.	Age (¹⁴ C years B.P.)	δ ¹³ C
<i>Canavan Knob diamicton</i>			
90-1, <i>Griselinia littoralis</i>	AA-9225	11,350 ± 90	-24.2
	A-6047	11,240 ± 100	-24.2
	Wk-1998	11,150 ± 160	-28.3
	Wk-1588	11,350 ± 60	-24.4
91-2, Compositae	A-6307	11,110 ± 130	-24.9
91-2A, <i>Dracophyllum</i> sp.	A-6308	11,230 ± 130	-24.4
91-2B, <i>Dracophyllum</i> sp.	A-6309	11,290 ± 150	-23.0
	Wk-2233	11,090 ± 70	-24.1
91-2C, <i>Dracophyllum</i> sp.	A-6310	11,340 ± 110	-25.0
91-2D, <i>Dracophyllum</i> sp.	A-6311	11,040 ± 90	-25.9
	Wk-2234	11,190 ± 60	-26.8
91-2E, <i>Leptospermum scoparium</i>	Wk-2235	11,150 ± 60	-25.5
91-2F, <i>Dracophyllum</i> sp.	Wk-2236	11,370 ± 190	-28.1
91-3A, <i>Dracophyllum</i> sp.	Wk-2237	11,200 ± 50	-28.0
91-3B, Compositae	Wk-2238	11,250 ± 70	-27.7
91-3C, <i>Metrosideros</i> sp.	Wk-2239	10,950 ± 100	-25.1
91-3E, <i>Leptospermum Scoparium</i>	A-6312	11,045 ± 85	-25.3
91-3F, <i>Weinmannia</i> sp.	A-6313	11,040 ± 70	-24.5
	Wk-2240	10,980 ± 90	-27.2
91-3G, <i>Weinmannia</i> sp.	Wk-2241	11,080 ± 60	-28.5
91-3H, Compositae	Wk-2242	11,225 ± 60	-27.2
91-3I, Compositae	AA-9514	10,980 ± 100	-25.8
	A-6314	10,830 ± 110	-25.8
91-3J, <i>Weinmannia</i> sp.	A-6315	11,255 ± 95	-24.5
91-3L, Compositae	Wk-2243	11,115 ± 90	-28.0
91-3M, <i>Metrosideros</i> sp.	A-6316	11,110 ± 110	-25.4
	Wk-2240	11,110 ± 90	-28.0
91-3N, Compositae	AA-9513	10,650 ± 100	-25.2
	A-6317	10,920 ± 90	-25.2
91-4, <i>Weinmannia</i> sp.	A-6318	11,520 ± 140	-24.1
	A-6593	11,250 ± 50	-24.1
	Wk-2245	11,365 ± 60	-24.1
92-1, <i>Dracophyllum</i> sp.	A-6707	11,520 ± 170	-23.8
92-2, <i>Fruschia excorticata</i>	A-6588	11,200 ± 120	-27.3
92-4, <i>Weinmannia racemose</i>	Wk-2352	10,800 ± 90	-25.8
92-5, <i>Olearia</i> sp.	Wk-2353	10,750 ± 100	-27.5
92-7, Basal organic silt	A-6589	11,740 ± 70	-28.6
<i>Surface wood, Franz Josef Glacier</i>			
92-13, <i>Griselinia littoralis</i>	Wk-2358	A.D. 1958–59 (114.92 ± 0.6%)	-24.2
92-14, <i>Griselinia littoralis</i>	Wk-2359	A.D. 1963 or 1975–76 (137.54 ± 0.74%)	-28.0
92-15, <i>Olearia</i> sp.	Wk-2360	A.D. 1963 or 1979–83 (129.28 ± 0.7%)	-26.2
92-16, <i>Metrosideros</i> sp.	Wk-2361	A.D. 1959–62 or post 1985 (121.87 ± 0.74%)	-25.6
<i>Surface wood, Fox Glacier</i>			
92-9, <i>Olearia</i> sp.	Wk-2354	living before A.D. 1954 (98.64 ± 0.6%)	-27.8
92-10, <i>Griselinia littoralis</i>	Wk-2355	living before A.D. 1954 (98.83 ± 0.6%)	-26.0
92-11, <i>Olearia</i> sp.	Wk-2356	living before A.D. 1954 (98.24 ± 0.6%)	-26.7
92-12, <i>Olearia</i> sp.	Wk-2357	A.D. 1958–59 (111.96 ± 0.66%)	-26.8

REFERENCES AND NOTES

- W. Dansgaard, J. W. C. White, S. J. Johnsen, *Nature* **339**, 532 (1989).
- T. C. Atkinson, K. R. Briffa, G. R. Coope, *ibid.* **325**, 587 (1987).
- U. Siegenthaler, U. Eicher, H. Oeschger, W. Dansgaard, *Ann. Glaciol.* **5**, 149 (1984).
- K. C. Taylor *et al.*, *Nature* **361**, 432 (1993).
- R. B. Alley *et al.*, *ibid.* **362**, 527 (1994).
- S. J. Lehman and L. D. Keigwin, *ibid.* **356**, 757 (1992).
- L. D. Keigwin, G. A. Jones, S. J. Lehman, E. A. Boyle, *J. Geophys. Res.* **96**, 16811 (1991).
- W. S. Broecker, G. Bond, M. Klas, G. Bonani, W. Wolfli, *Paleoceanography* **5**, 469 (1990).
- R. Alley *et al.*, *Eos* **50**, 587 (1993).
- B. K. Linsley and R. C. Thunell, *Paleoceanography* **5**, 1025 (1990).
- H. R. Kudrass, H. Erlenkeuser, H. Volbrecht, W. Weiss, *Nature* **349**, 406 (1991).
- N. Kallel *et al.*, *Oceanol. Acta* **11**, 369 (1988).
- B. P. Flower and J. P. Kennett, *Paleoceanography* **5**, 1009 (1990).
- L. D. Keigwin and G. A. Jones, *ibid.*, p. 1009.
- J. Jouzel *et al.*, in *The Last Deglaciation: Absolute and Radiocarbon Chronologies*, E. Bard and W. S. Broecker, Eds. (Springer-Verlag, New York, 1992), pp. 230–266.
- N. Roberts *et al.*, *Nature* **366**, 146 (1993).
- T. J. H. Chinn and M. Kirkbride, *Guidebook for the Post Symposium Glacier Tour of New Zealand*. (International Glaciological Society Symposium on Ice Dynamics, Hobart, Australia, 1988).
- R. P. Suggate, *J. Glaciol.* **1**, 422 (1950).
- G. Warren, *Sheet 17 Hokitika Geologic Map, N.Z., 1:250,000* (Division of Scientific and Industrial Research, Wellington, New Zealand, ed. 1, 1967).
- R. P. Suggate, *N.Z. Geol. Surv. Bull.* **77**, 1 (1965).
- R. P. Suggate, Ed., *The Geology of New Zealand* (Government Printer, Wellington, New Zealand, 1978), two volumes.
- _____, *New Zealand Geological Survey Record 7* (Division of Scientific and Industrial Research, Wellington, New Zealand, 1985), p. 22.
- _____, and N. T. Moar, *N.Z. J. Geol. Geophys.* **13**, 742 (1970).
- Deposits of the Otiran Glaciation (the last glaciation) make up the Loopline, Larrikins (equal to the Okarito), and Moana formations on the northwestern flank of the Southern Alps (17–20). The formations are mapped over wide areas and hence reflect the overall behavior of the Southern Alps glacier systems. Each formation includes deposits of a single broad glacier advance. The Kumara 2₂ advance is associated with the Larrikins and Okarito formations; it occurred 18,000 to 22,300 ¹⁴C years B.P. (19–21). The Kumara 3 fluctuation is recorded by the Moana Formation. Locally, two closely spaced Kumara 3 advances are noted (19, 21). The Kumara 3₂ advance occurred 14,000 to 15,000 ¹⁴C years B.P. (21). Widespread glacier recession was under way about 14,000 ¹⁴C years B.P. (18, 19, 21).
- P. Wardle, *N.Z. Bot.* **11**, 349 (1973).
- _____, *ibid.* **16**, 147 (1978).
- J. H. Mercer, *N.Z. Geol. Geophys.* **31**, 95 (1988).
- Previous dates of wood in the wood-bearing diamicton from the Canavan Knob stratigraphic section (25–27) yielded some radiocarbon dates that were older than those in Table 1. For example, four samples from the same piece of wood yielded discordant radiocarbon ages of 11,500 ± 200 years B.P. (NZ6923A); 11,700 ± 200 years B.P. (NZG923A); 12,100 ± 275 years B.P. (GX-10053); and 12,500 ± 120 years B.P. (Beta-12607) (27). From what we believe to be the same

piece of wood (sample 90-1 in the table) from Mercer's photograph (27), we obtained concordant radiocarbon ages from three laboratories of $11,350 \pm 90$ (AA-9225); $11,240 \pm 100$ (A-6047); $11,150 \pm 160$ (Wk-1998); and $11,350 \pm 50$ years B.P. (Wk-1588); these ages agree with all others in Table 1 and thus we consider them to be accurate. We cannot explain the discrepancies with the dates from Mercer (27). Also, Mercer implied that some of the wood was in place. From extensive excavations, we conclude that all the wood pieces in Canavan Knob section were transported.

- 29. P. Wardle, personal communication.
- 30. L. R. Basher and M. McSaveney, *R. Soc. N.Z.* **19**, 263 (1989).
- 31. T. J. H. Chinn, *U.S. Geol. Surv. Prof. Pap.* **1386-H**, H25 (1989).
- 32. J. C. Duplessy, in *Global Changes of the Past*, R. S. Bradley, Ed. (University Center for Atmospheric Research, Office for Interdisciplinary

- Earth Studies, Denver, CO, 1989), pp. 341-355.
- 33. S. Björck and P. Möller, *Quat. Res.* **28**, 1 (1987).
- 34. J. Mangerud, B. G. Andersen, E. Larsen, *Terminat. Pleistocene* **5**, 1 (1992).
- 35. J. T. Hollin and D. H. Schilling, in *The Last Great Ice Sheets*, G. H. Denton and T. J. Hughes, Eds. (Wiley-Interscience, New York, 1981), pp. 179-206.
- 36. Funded by the National Science Foundation and the National Geographic Society. C. Schlüchter and H. Conway helped interpret the stratigraphy and radiocarbon samples. We appreciate the cooperation of officials of Westland National Park. We thank R. Kalin and C. Eastoe; A. G. Hogg; and T. M. Jull for radiocarbon analyses. R. N. Patel identified the wood samples. We thank C. Claperton, G. Jacobson, P. Wardle, R. P. Suggate, S. Björck, T. Chinn, and M. McGlone for helpful comments on the manuscript.

20 December 1993; accepted 25 April 1994

Implications for Mantle Dynamics from the High Melting Temperature of Perovskite

Peter E. van Keken,* David A. Yuen, Arie P. van den Berg

Recent studies have implied that (Mg,Fe)SiO₃-perovskite, a likely dominant mineral phase in the lower mantle, may have a high melting temperature. The implications of these findings for the dynamics of the lower mantle were investigated with the use of numerical convection models. The results showed that low homologous temperatures (0.3 to 0.5) would prevail in the modeled lower mantle, regardless of the effective Rayleigh number and internal heating rates. High-temperature ductile creep is possible under relatively cold conditions. In models with low rates of internal heating, local maxima of viscosity developed in the mid-lower mantle that were similar to those obtained from inversion of geoid, topography, and plate velocities.

Recent experimental results have indicated that the melting temperature of (Mg,Fe)SiO₃-perovskite in the lower mantle may be much higher than earlier estimates suggested (1, 2) (Fig. 1). This high melting temperature, increasing from 2500 K at the top of the lower mantle to an extrapolated value of approximately 8000 K at the core-mantle boundary (CMB), would have a profound influence on the flow processes in the lower mantle. We investigated steady-state convection models in order to study the thermal structure and viscosity distribution in the lower mantle with a rheology compatible with the high-temperature melting curve.

For modeling purposes, we linearized the estimates of the melting temperatures from (1), according to

$$T_m = 2000 + 2000A_1z/z_1 \quad z \geq z_0 \quad (1)$$

where z_1 is the depth of the CMB (3000 km), z_0 is 670 km, and the parameter A_1 is varied between 2 and 3. $A_1 = 3$ gives a melting curve that falls within the range indicated by the three methods of extrapolation (Fig. 1). We set up parameters for the nondimensional viscosity using an Arrhenius type of creep law under Weertman's assumption on the basis of homologous temperature (3) as follows:

$$\eta = \exp\left(\frac{A}{T_0 + T}\right) \exp\left(-\frac{A_0}{T_0}\right) \quad (2)$$

where

$$A = \begin{cases} A_0 \left[1 + A_1 \frac{(z - z_0)}{(z_1 - z_0)} \right] & z \geq z_0 \\ A_0 & z < z_0 \end{cases}$$

($z \geq z_0$ refers to the lower mantle; $z < z_0$ refers to the upper mantle). The parameter A can be seen as an activation temperature that increases linearly with depth, following the melting relation (Eq. 1). A_0 is used to scale the maximum viscosity contrast $\Delta\eta$ between the top and bottom of the mantle, which in most cases is

taken to be $\Delta\eta = 1000$ (4). The temperature T_0 is arbitrarily chosen to be the nondimensionalized lithospheric temperature of 800 K ($T_0 = 0.2$). Varying this parameter will have some consequences for the viscosity distribution in the upper mantle but will not have a strong influence on the viscosity in the lower mantle, which is governed mainly by the increase in melting temperature (Eq. 1) and by the factor A_0 in Eq. 2. The nondimensional equations for momentum and energy are solved for an incompressible Boussinesq fluid at infinite Prandtl number in a two-dimensional Cartesian geometry with an aspect ratio of 1 (5). The temperature is scaled to the temperature difference across the layer, on the basis of an estimate of temperature at the CMB of $T_{CMB} = 4000$ K (6). The viscosity is scaled to be $\eta = 1$ at the surface.

For a surface Rayleigh number $Ra_s = 10^4$ and viscosity contrast $\Delta\eta = 1000$, we first considered the case where melting temperature is independent of depth (Fig. 2A). The mantle was nearly isoviscous, apart from a viscosity contrast of 1000 across the upper thermal boundary layer. At constant temperature, increasing A_1 gave only a moderate viscosity increase, from a factor of about 20 at $A_1 = 2$ to a factor of 50 at $A_1 = 3$. However, increasing the melting temperature gradient in the lower mantle decreased the internal temperature substantially, and the combined effect increased both the lateral and vertical viscosity contrasts in the lower mantle by several orders of magnitude (Fig. 2, B and C). Deep in the lower mantle, the viscosities varied by four orders of magnitude. A large part of the interior became very cold with increasing A_1 , whereas the rising plume was broadened (Fig. 2C). Flow fields were on the order of 10 to 1000 times lower than in the

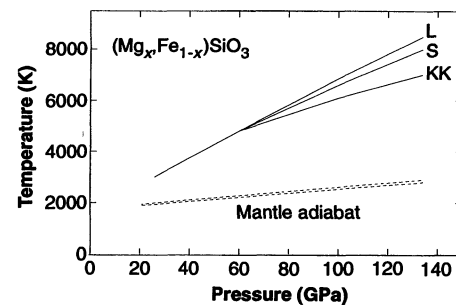


Fig. 1. Melting curve of (Mg,Fe)SiO₃-perovskite, after Zerr and Boehler (1). Melting data were obtained between 25 and 62.5 GPa. The solid lines show the fit to the data and extrapolation using Lindemann's law (L) and the Kraut-Kennedy (KK) and Simon (S) melt relations (1). The dashed lines indicate a range of estimates for temperatures in an adiabatic mantle (1).

P. E. van Keken, Army High Performance Computing Research Center, University of Minnesota, 1100 Washington Avenue South, Minneapolis, MN 55415, USA.

D. A. Yuen, Minnesota Supercomputer Institute, University of Minnesota, 1200 Washington Avenue South, Minneapolis, MN 55415, USA.

A. P. van den Berg, Department of Theoretical Geophysics, Institute of Earth Sciences, Postal Box 80.021, 3508 TA, Utrecht, Netherlands.

*To whom correspondence should be addressed.